The Astrophysical Journal, 891:86 (8pp), 2020 March 1 https://doi.org/10.3847/1538-4357/ab7234

Kinetic Models of Tangential Discontinuities in the Solar Wind

T. Neukirch[1], I. Y. Vasko[2,3], A. V. Artemyev[3,4], and O. Allanson[5]
[1] School of Mathematics and Statistics, University of St Andrews, St Andrews KY16 9SS, UK; tn3@st-andrews.ac.uk
[2] Space Sciences Laboratory, University of California, Berkeley, CA 94720, USA
[3] Space Research Institute of Russian Academy of Sciences, Moscow, Russia
[4] Institute of Geophysics and Planetary Sciences, University of California, Los Angeles, CA 90095, USA
[5] Space and Atmospheric Electricity Group, Department of Meteorology, University of Reading, Reading, RG6 6BB, UK
Received 2019 November 20; revised 2020 January 28; accepted 2020 January 30; published 2020 March 6

Abstract

Kinetic-scale current sheets observed in the solar wind are frequently approximately force-free despite the fact that their plasma β is of the order of one. In situ measurements have recently shown that plasma density and temperature often vary across the current sheets, while the plasma pressure is approximately uniform. In many cases these density and temperature variations are asymmetric with respect to the center of the current sheet. To model these observations theoretically we develop in this paper equilibria of kinetic-scale force-free current sheets that have plasma density and temperature gradients. The models can also be useful for analysis of stability and dissipation of the current sheets in the solar wind.

Unified Astronomy Thesaurus concepts: Solar wind (1534); Interplanetary discontinuities (820); Interplanetary magnetic fields (824)

1. Introduction

The early in situ measurements in the solar wind indicated the ubiquity of magnetic field discontinuities or, equivalently, current sheets with spatial scales below a few tens of ion thermal gyroradii or ion inertial lengths (e.g., Burlaga et al. 1977; Tsurutani & Smith 1979; Lepping 1986). The magnetic reconnection within these kinetic-scale structures may provide ion and electron heating (e.g., Osman et al. 2011; Gosling 2012; Pulupa et al. 2014), though the overall contribution of the current sheets to the solar wind heating is unknown (e.g., Cranmer et al. 2009). The disruption of the kinetic-scale current sheets via the magnetic reconnection is potentially a mechanism resulting in the spectral break of the magnetic field turbulence spectrum at ion scales (e.g., Franci et al. 2017; Mallet et al. 2017; Vech et al. 2018). The mechanisms responsible for formation of the current sheets include Alfvén wave steepening (e.g., Medvedev et al. 1997) and the natural appearance of sheet-like structures in the course of development of the turbulence cascade (e.g., Greco et al. 2009, 2016; Franci et al. 2017).

The early in situ measurements focused on classifying the current sheets in terms of tangential and rotational discontinuities based on the analysis of the magnetic field component perpendicular to the current sheet plane (e.g., Tsurutani & Smith 1974; Burlaga et al. 1977; Lepping 1986). However, the estimates of the fraction of tangential and rotational discontinuities in the solar wind are still controversial (e.g., Knetter et al. 2004; Neugebauer 2006; Artemyev et al. 2019b). The in situ measurements unambiguously showed that current sheets in the solar wind are often approximately one-dimensional and force-free, i.e., the current density is mostly parallel to the magnetic field and the magnetic field rotates across a current sheet, while its magnitude remains constant (e.g., Burlaga et al. 1977; Lepping 1986; Neugebauer 2006; Paschmann et al. 2013). Recent statistical analyses (Artemyev et al. 2018, 2019b) have shown that the plasma density n and ion and electron temperatures $T_{i,e}$ typically vary across a current sheet. In these analyses it was also shown that the density and temperature variations are anticorrelated $\Delta T_{i,e}/T_{i,e} \propto -\Delta n/n$, so that the plasma pressure is essentially uniform across the current sheets as required by the pressure balance.

Within the large number of known one-dimensional kinetic current sheet models (e.g., Lemaire & Burlaga 1976; Bobrova & Syrovatskiĭ 1979; Roth et al. 1996; Kocharovsky et al. 2010; Panov et al. 2011), the most relevant to the solar wind observations mentioned above are the recently developed models of force-free current sheets representing tangential (Harrison & Neukirch 2009a; Wilson & Neukirch 2011; Allanson et al. 2015) and rotational (Artemyev 2011; Vasko et al. 2014) discontinuities. In these kinetic models of both force-free tangential and rotational discontinuities the plasma density and temperature are uniform across the current sheet.

We remark that there is a much broader class of collisionless tangential discontinuity models (Roth et al. 1996) that can in principle be used to describe magnetic fields of solar wind discontinuities (De Keyser et al. 1996; De Keyser & Roth 1997) and does even allow for the inclusion of plasma velocity shear (De Keyser et al. 1997, 2013), which is observed for some solar wind discontinuities (De Keyser et al. 1998; Paschmann et al. 2013; Artemyev et al. 2019b).

These models start from specifying the dependence of the distribution functions on the constants of motion and have been developed to give a detailed description different plasma populations in magnetic current sheets (Roth et al. 1996). When starting from specifying the particle distribution functions any self-consistent model of a collisionless configuration has to be completed by solving Maxwell's equations. With the form of the distribution functions used for a detailed description of current sheets (see, e.g., the model-data comparison in De Keyser et al. 1996, 1997) it is usually not possible to obtain analytical solutions for the electromagnetic fields and hence these have to be determined using numerical methods. This in turn implies that the exact spatial variation of the particle densities, the pressure, and the temperature is only available after the numerical calculation of the electromagnetic fields has been carried out.

In this paper we use a different approach, mainly for two reasons. First, as already mentioned above, the magnetic field configuration of many of the current sheets observed in the solar wind is observed to be force-free to a good approximation (e.g., Artemyev et al. 2019a). For one-dimensional tangential discontinuities this directly implies that the magnetic field strength $|\boldsymbol{B}|$ and the plasma pressure do not vary across the discontinuity (see e.g., Harrison & Neukirch 2009b; Neukirch et al. 2018). This puts additional constraints on the possible dependence of the particle distribution functions on the constants of motion and makes finding such distribution functions for force-free magnetic field configurations non-trivial. As a number of self-consistent distribution functions for the force-free version of the Harris sheet (Harris 1962) have been found (e.g., Harrison & Neukirch 2009a; Neukirch et al. 2009; Wilson & Neukirch 2011; Allanson et al. 2015; Kolotkov et al. 2015; Wilson et al. 2017, 2018), we use one of those force-free distribution functions as a starting point for the investigation in this paper.

Moreover, second, in the case we consider in this paper the process of determining appropriate distribution functions for a force-free magnetic tangential discontinuity starts from a known electromagnetic field configuration (here the force-free Harris sheet) and one determines compatible distribution functions that lead to a self-consistent equilibrium by solving this "inverse" problem (see, e.g., Allanson et al. 2016, 2018; Neukirch et al. 2018). Starting from an analytically known magnetic field configuration and corresponding distribution functions as a starting point of the investigation allows us more direct control. An additional advantage of a completely analytical approach could be that it usually simplifies the implementation of the kinetic equilibrium as initial conditions in numerical simulations using, for example, particle-in-cell (PIC) codes.

The crucial point is that none of the currently known collisionless force-free current sheet models is capable of describing the recently observed nonuniform density and temperature profiles in the solar wind current sheets. Thus, it is our main motivation to develop analytical kinetic models of force-free current sheets that include the observed features. From a more theoretical point of view, the development of analytical kinetic current sheet models including the observed gradients will also simplify further investigations of their dynamics. For example, it is known that the stability of current sheets is rather sensitive to the initial equilibrium configuration (e.g., Pucci et al. 2018). Moreover, PIC simulations have recently shown that the nonlinear evolution of the reconnection process and particle acceleration is strongly dependent on the presence of the guide field and plasma density and temperature gradients across the current sheets (e.g., Wilson et al. 2016; Lu et al. 2019a).

In this paper we present observations of the solar wind current sheets with plasma density and temperature gradients and develop a class of collisionless force-free equilibrium models that incorporate the observed (asymmetric) variations of the plasma density and temperature.

2. Observations

We present observations of current sheets by the *ARTEMIS* spacecraft, which probes the solar wind at a few tens of Earth radii upstream of the Earth's bow shock (Angelopoulos 2011). We use the magnetic field measurements with temporal resolution of 5 vectors per second (Auster et al. 2008) and measurements of electron density and temperature available at 4 s cadence (all plasma parameters are measured by electrostatic analyzers on board *ARTEMIS*, see McFadden et al. 2008).

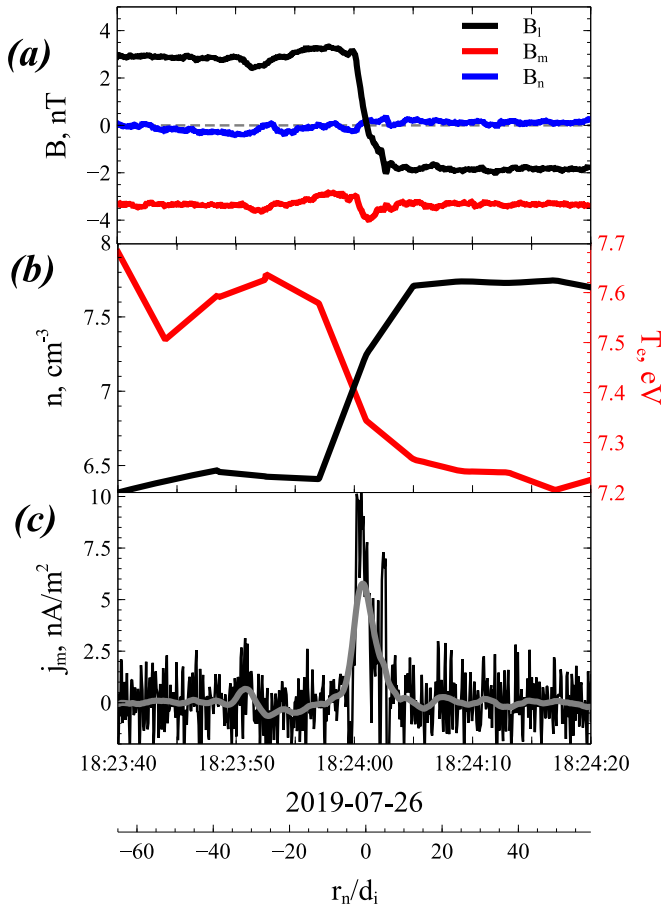

Figure 1. Example of a current sheet crossing by *ARTEMIS* spacecraft: (a) three magnetic field components in the local coordinate system (Sonnerup & Cahill 1968) with the additional constraint $\langle B_n \rangle = 0$ (see Section 8.2.6 in Sonnerup & Scheible 2000), (b) electron density and temperature measurements, and (c) current density profile (gray color shows smoothed profile). Bottom horizontal axis shows the spatial coordinate across the sheet (normalized on the ion inertial length, d_i).

Figure 1 presents an example of a particular current sheet observed aboard *ARTEMIS*. Panel (a) presents the magnetic field in the coordinate system (l, m, n) determined using the minimum variance analysis (MVA; Sonnerup & Cahill 1968). The magnetic field component B_n is perpendicular to the current sheet plane, B_l reverses the sign across the current sheet, B_m is the so-called guide field. In a 1D approximation all variables vary across the current sheet that is along the normal $\boldsymbol{n}$. Panel (a) shows that the current sheet is approximately force-free, because $B_l^2 + B_m^2 \approx \text{const}$. For the single spacecraft measurements the determination of the normal $\boldsymbol{n}$ is generally not sufficiently accurate (e.g., Horbury et al. 2001; Knetter et al. 2004) to separate rotational and tangential discontinuities. Thus, we assume that the observed discontinuity is tangential and apply an additional constraint to the local coordinate system, namely $\langle B_n \rangle = 0$ (see Section 8.2.6 in Sonnerup & Scheible 2000). Panel (b) shows that the plasma density and electron temperature variations across the current sheet are anticorrelated. The plasma density increases across the current sheet by about 20%, while the electron temperature decreases

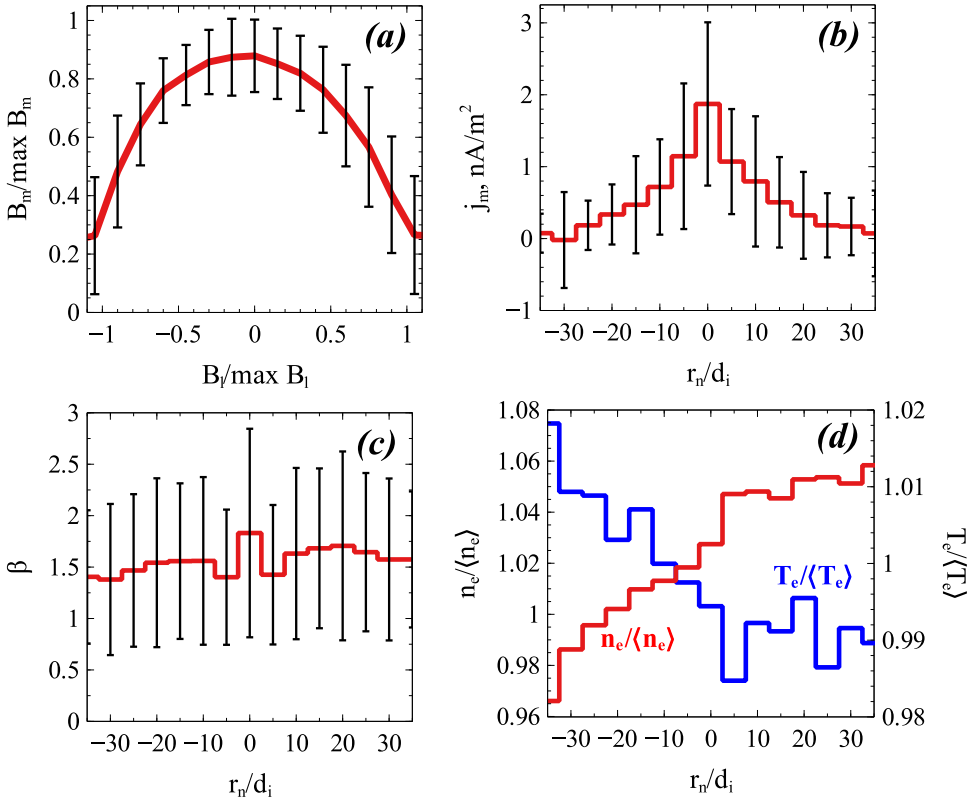

Figure 2. Average profiles of magnetic field, current density, and plasma characteristics for a data set of ∼200 discontinuities observed by the *ARTEMIS* spacecraft in the near-Earth solar wind (see details of the data set in Artemyev et al. 2019a). The main criterion of discontinuity selection to the data set is the peak current density exceeding 1 nA m^{-2}. Black error bars show the standard deviation. In each case, electron densities and temperatures are normalized by the average value across the discontinuity. Orientation of r_n is chosen to have $dn_e/dr_n > 0$ for all selected discontinuities.

by about 5%. *ARTEMIS* measurements of the ion temperature in the solar wind are much less accurate than electron temperature measurements. The assumption of the pressure balance across the current sheet suggests that the ion temperature should also decrease across the current sheet by a few tens of percent. Because the Taylor hypothesis applies for the current sheets in the solar wind, we can estimate the current densities $j_l \propto -dB_m/dt$ and $j_m \propto dB_l/dt$ (see Artemyev et al. 2019a for details). Panel (c) shows that the current density reaches values of 10 nA m^{-2}, which is comparable to the highest current densities in the solar wind (e.g., Podesta 2017). The use of the Taylor hypothesis allows translating the observations in time into space. The spatial axis in Figure 1 shows that the current sheet is an ion-scale structure with the thickness of a few ion inertial lengths or, equivalently, a few hundred kilometers. To demonstrate that the current sheet in Figure 1 is not exceptional, we use a data set of more than 400 current sheets collected by the *ARTEMIS* spacecraft over two years of observations (see Artemyev et al. 2019a for details).

Figure 2 presents the averaged properties of the selected current sheets. Panel (a) shows the current sheets in the solar wind typically have a half-ring B_m versus B_l. This is equivalent to the statement that ion-scale current sheets in the solar wind are predominantly force-free, i.e., $B_m^2 + B_l^2 \approx$ const. Panel (b) shows that the B_l reversal across the current sheet corresponds to the current density $j_m \sim 1$ nA m^{-2} localized within about 10 ion inertial lengths. Panel (c) shows that the plasma beta, $\beta = 8\pi p/B^2$, is typically about unity and does not vary across the current sheets in accordance with the force-free nature of the current sheets. Panel (d) shows that though β is approximately uniform across the current sheets, there are clearly variations of the plasma density and electron temperature. Statistically, the plasma density varies by about 10%, while the electron temperature varies by about 3% across the current sheet.

Although there are kinetic current sheet models that are sufficiently flexible to describe a large variety of tangential discontinuities (see, e.g., the review by Roth et al. 1996 and references therein), these models generally require a numerical solution of Maxwell's equations to achieve self-consistency. This complicates the matching of these models to the observations, in particular, with regards to the additional constraints that have to be satisfied by distribution functions for force-free collisionless current sheets. Therefore we will start from a kinetic current sheet model that is completely analytical and already satisfies the force-free condition. However, there are currently no simple analytical kinetic current sheet models that incorporate all of the observed features: (1) the force-free current sheet with spatial scales of a few ion inertial lengths and β of the order of unity; (2) anticorrelated plasma density and temperature variations across the current sheet. In the next section we develop kinetic models for such current sheets assuming that they are tangential in nature, that is $B_n = 0$.

We should mention that not all the discontinuities that were observed (and included in our statistics) are tangential, but that distinguishing observationally between tangential and rotational discontinuities is not a well resolved problem (see the discussion in Neugebauer 2006). The data set presented in Figure 2 has been collected by the two *ARTEMIS* probes, whereas at least four-spacecraft observations are required for an

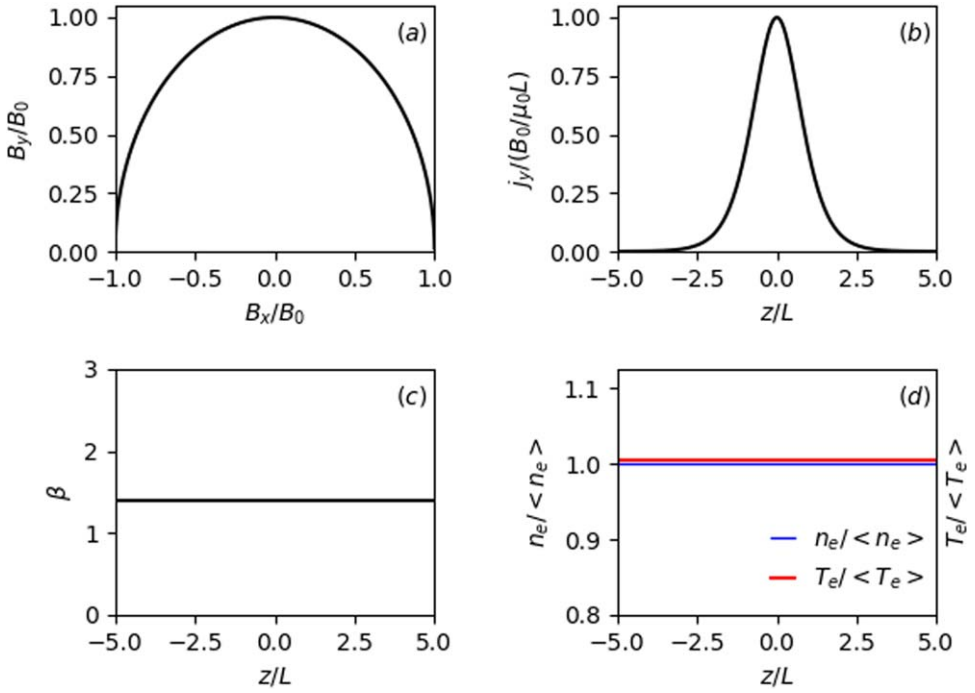

Figure 3. Summary of the macroscopic properties of the current sheet models developed by Harrison & Neukirch (2009b): (a) the half-ring B_x vs. B_y shape is due to $B_x^2 + B_y^2 = B_0^2$; (b) the profile of the y-component of the current density (c, d) the plasma β is generally above unity, while the plasma density and electron and ion temperatures are uniform across the current sheet.

accurate determination of the local coordinate system and estimation of B_n (Knetter et al. 2004). Therefore, in this paper we focus on modeling tangential discontinuities and leave the question of the relative percentage of tangential versus rotational discontinuities within the total amount of solar wind discontinuities to future investigations.

Independently of the classification of the discontinuities, the observations of these plasma structures in the solar wind are often associated with measurements of plasma shear flow (De Keyser et al. 1998; Paschmann et al. 2013; Artemyev et al. 2019a). This shear flow, which is related to the cross-field plasma (both ion and electron) velocity, can result in the generation of polarization electric fields (e.g., Roth et al. 1996; De Keyser et al. 2013) that are enhanced by plasma pressure gradients across the discontinuities (e.g., Yoon & Lui 2004; Lu et al. 2019b). However, there are no such gradients in force-free discontinuities. Moreover, some population of these discontinuities have the main magnetic field reversal along the solar wind flow, i.e., the plasma shear flow is along the magnetic field and there is almost no cross-field shear flow. For this type of discontinuity the effect of the polarization electric field is negligible. In this paper we will focus on the theoretical description of this type of discontinuity and will not consider a finite electric field. A more general case could, for example, be described in future studies following the approach from De Keyser et al. (2013).

3. Kinetic Model of a Force-free Tangential Discontinuity

In this section the local coordinate system $(\boldsymbol{l}, \boldsymbol{m}, \boldsymbol{n})$ is denoted (x, y, z). We consider a one-dimensional current sheet with the magnetic field $\boldsymbol{B} = B_x(z)\boldsymbol{e}_x + B_y(z)\boldsymbol{e}_y$. The development of a stationary kinetic current sheet model requires us to provide a class of electron and ion distribution functions $F_{i,e}(\boldsymbol{v}, z)$, which would result in the current density $\boldsymbol{j} = j_x(z)\boldsymbol{e}_x + j_y(z)\boldsymbol{e}_y$ consistent with the magnetic field $\boldsymbol{B}$, and the desired spatial distribution of the plasma density and ion and electron temperatures across the current sheet. The particle distribution functions, being solutions of the Vlasov equation, can be written as functions of the integrals of particle motion (e.g., Schindler 2007). In the considered one-dimensional current sheet there are three integrals of particle motion: the total energy $H_s = m_s\boldsymbol{v}^2/2 + q_s\Phi$ and generalized momenta $p_{xs} = m_s v_x + q_s A_x/c$ and $p_{ys} = m_s v_y + q_s A_y/c$, where $\Phi(z)$ is the electrostatic potential, $\boldsymbol{A} = A_x(z)\boldsymbol{e}_x + A_y(z)\boldsymbol{e}_y$ is the vector potential, m_s and q_s are particle mass and charge, $s = i, e$ correspond to ions and electrons ($q_i = -q_e \equiv e$).

Figure 3 illustrates the macroscopic quantities consistent with the class of kinetic models of force-free current sheets with the magnetic field $B_x(z) = B_0\tanh(z/L)$ and $B_y(z) = B_0\cosh^{-1}(z/L)$ developed by Harrison & Neukirch (2009a). In that class of models $B_x^2 + B_y^2 = B_0^2$, the plasma density and particle temperatures are uniform across the current sheet, and the model parameters are chosen in such a way that the electrostatic field vanishes identically, $\Phi(z) = 0$. The plasma β is above unity in the original class of Harrison & Neukirch (2009a) models, but β can be arbitrary in more generalized models (see Neukirch et al. 2018 for a review). The simplest example from that class of models is the one with the ion distribution function given by the Maxwellian distribution, $F_{0i}(\boldsymbol{v}, z) = n_0(m_i/2\pi T_i)^{3/2}\exp(-H_i/T_i)$, and electron distribution function given as follows

$$F_{0e}(\boldsymbol{v}, z) = n_0(1+b)^{-1}\left(\frac{m_e}{2\pi T_e}\right)^{3/2}\exp(-H_e/T_e)$$
$$\cdot\left[b + \exp(u_0 p_{ye}/T_e)\exp(-m_e u_0^2/2T_e)\right.$$
$$\left.-\frac{1}{2}\cos(u_0 p_{xe}/T_e)\exp(m_e u_0^2/2T_e)\right],$$

where n_0 is the plasma density, T_e and T_i are electron and ion temperatures (here and in the remainder of this paper we absorb the Boltzmann constant factor, k_B into the temperature), u_0 is related to B_0 and L by the relations $en_0u_0 = -cB_0/4\pi L$ and $B_0L = -2T_e/eu_0$. This implies that $L^2 = cT_e/2\pi e^2 n_0 u_0^2$. The electron temperature determines the amplitude of the magnetic field, $B_0^2 = 8\pi n_0 T_e$. The parameter b sets the density of the background electron population not contributing to the current density, it has to be large enough to keep the electron velocity distribution function positive. In what follows we generalize the models developed by Harrison & Neukirch (2009a) to have the asymmetric distribution of the plasma density across the current sheet similar to that in Figures 1 and 2.

The models of force-free current sheets with asymmetric plasma density profiles can be developed within a rather wide class of particle velocity distribution functions: $F_s = F_{0s}(H_s, p_{xs}, p_{ys}) + \Delta F_s(H_s, p_{xs})$, where F_{0s} is, for example, the class of distribution functions suggested by Harrison & Neukirch (2009b), while $\Delta F_s(H_s, p_{xs})$ corresponds to additional electron and ion populations. In principle, F_{0s} can be any distribution function consistent with the magnetic field profile (e.g., Allanson et al. 2015, 2016; Kolotkov et al. 2015; Wilson et al. 2017, 2018). The distribution function of the additional populations should be chosen so that they provide no contribution to the current density, $\int v_x \Delta F_s d^3\boldsymbol{v} = 0$, but contribute to the density $\int \Delta F_s(H_s, p_{xs}) d^3\boldsymbol{v} = \Delta n_s(A_x)$, where Δn_s should be an odd function of A_x that is $\Delta n_s(-A_x) = -\Delta n_s(A_x)$. In that case the magnetic field remains identical to that in the models of Harrison & Neukirch (2009a), while the electron density distribution will be asymmetric across the current sheet, because $A_x(z) = B_0 L \arctan[\sinh(z/L)]$ is asymmetric with respect to $z = 0$. Because the magnetic field configuration remains force-free that is $B^2 = \text{const}$, the pressure balance across the CS $p_{zz} + B^2/8\pi = \text{const}$ results in a constant zz-component of the pressure tensor, $p_{zz} = \text{const}$. For a nonuniform plasma density the variation of the temperature T_{zz} across the current sheet is anticorrelated with the density variation.

One of the simplest choices of the velocity distribution functions of the additional populations is $\Delta F_s = g_s(H_s) u_0 p_{xs}/T_e$, where $g_s(H_s)$ should satisfy $\int v_x^2 g_s(H_s) d^3\boldsymbol{v} = 0$. The class of functions $g_s(H_s)$ satisfying the latter condition is rather broad, while a particular example is

$$g_s = \delta n_s \left(\frac{m_s}{2\pi T_s}\right)^{3/2} \frac{\kappa_s^{5/2} e^{-\kappa_s H_s/T_s} - \tilde{\kappa}_s^{5/2} e^{-\tilde{\kappa}_s H_s/T_s}}{\kappa_s - \tilde{\kappa}_s},$$

where δn_s, κ_s, and $\tilde{\kappa}_s$ are free parameters. The number of free parameters can be reduced by taking the limit $\tilde{\kappa}_s \to \kappa_s$, which leads to the following class of ΔF_s

$$\Delta F_s = \delta n_s \left(\frac{\kappa_s m_s}{2\pi T_s}\right)^{3/2} \left(\frac{5}{2} - \frac{\kappa_s H_s}{T_s}\right) e^{-\kappa_s H_s/T_s} \frac{u_0 p_{xs}}{T_s}.$$

The additional particle density is given by

$$\Delta n_s = -\frac{q_s}{e}\delta n_s \exp(-q_s\kappa_s\beta_s\Phi)(1 - q_s\kappa_s\beta_s\Phi)\frac{2A_x}{B_0 L}. \quad (1)$$

The quasi-neutrality condition $\sum_s q_s n_s = 0$ has the solution $\Phi = 0$, if we let $\delta n_i = -\delta n_e$.

The expression in Equation (3) is a relatively simple member of a wider class of functions with the desired property that they contribute to the particle density, but not to the current density (if $\Phi = 0$). We remark that by choosing parameters appropriately it is always possible to ensure that the total DF, $F_s + \Delta F_s$, is positive definite.

With $\Phi = 0$, $q_e = -e$, and $q_i = e$ (and defining $\delta n_e = \epsilon n_0$) the additional density term is given by

$$\Delta n_s = \Delta n = \epsilon n_0 \frac{2A_x}{B_0 L}. \quad (2)$$

Because $A_x(z)$ is asymmetric with respect to z, Δn_s introduces the desired density asymmetry across the current sheet. If we define the temperature via the equation $p_{zz,e} = k_B T_e n_e$, the temperature will also be asymmetric due to the pressure remaining constant, as found in the observations (Artemyev et al. 2019b).

In order to construct a realistic example we now assume that $L/d_i = 10$ (the ratio of the current sheet width to the ion inertial length), $\beta_p = 1.4$, $T_e/T_i = 1.0$, and $m_i/m_e = 1836$. We then find that $u_0/v_{\text{th},e} = \sqrt{2m_e/m_i\beta_p}\, d_i/L \approx -3.9 \cdot 10^{-3}$. Using $\kappa_e = \kappa_i = 1.1$ and $\epsilon = 0.05$, both distribution functions can be shown to be positive. We show example plots of the variation of the full electron and the ion distribution functions with v_x (for fixed values of z, v_y, and v_z) in Figures 4 and 5. Due to the relatively small value of $u_0/v_{\text{th},e}$, the difference between the total electron and ion distribution functions is also very small. In the same figures we also show how ΔF_s varies with v_x.

In Figure 6 we show the resulting modified density and temperature profiles for the same parameter values that were used for the distribution function plots. As desired the density and temperature profiles show the general behavior that is also seen in the observation shown in Figure 2

The structure of the distribution function in velocity space is seen to be very close to a Maxwellian distribution function (see Figures 4 and 5). This structure suggests that the distribution functions presented in this paper are likely to be stable to small perturbations (e.g., see standard stability arguments by Gardner 1963; Krall & Trivelpiece 1973).

4. Discussion and Conclusion

Recent spacecraft observations have shown that current sheets in the solar wind frequently exhibit nonsymmetric and anticorrelated electron density and temperature distributions with respect to the current sheet center (Artemyev et al. 2018). The origin and effects of these features on the stability of the current sheets in the solar wind remains unknown, partly due to the absence of kinetic models that could be used in the stability analysis. Self-consistent kinetic models of force-free current sheets have only been developed relatively recently (e.g., Harrison & Neukirch 2009a) and in these models the plasma and temperature distributions are uniform.

In this paper we have demonstrated that by adding a suitable further term to the distribution function of Harrison & Neukirch (2009a) it is possible to generate self-consistent kinetic equilibria which have asymmetric spatial profiles of particle density and temperature, while retaining the macroscopic current sheet equilibrium unchanged. We have presented an illustrative example which showed that for parameter values that are typical for solar wind current sheets observed at 1 au, one can easily find self-consistent particle distribution functions giving rise to macroscopic spatial variations in particle density

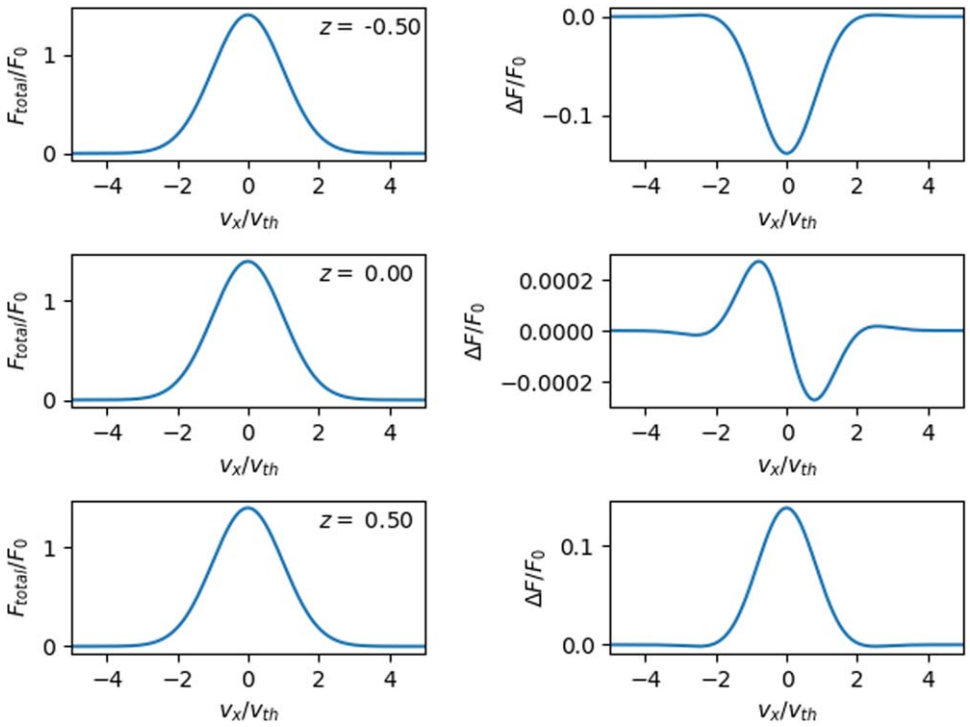

Figure 4. In the left column the dependence of the total electron DF $F_{0e} + \Delta F_e$ on v_x (for $v_y = v_z = 0$) is shown at three different positions: $z/L = -0.5$ (top row), $z/L = 0.0$ (middle row), and $z/L = 0.5$ (bottom row). The right column shows the same plots for ΔF_e alone. Here $\epsilon = 0.05$ and $u_0/v_{\mathrm{th},e} = -3.9 \cdot 10^{-3}$.

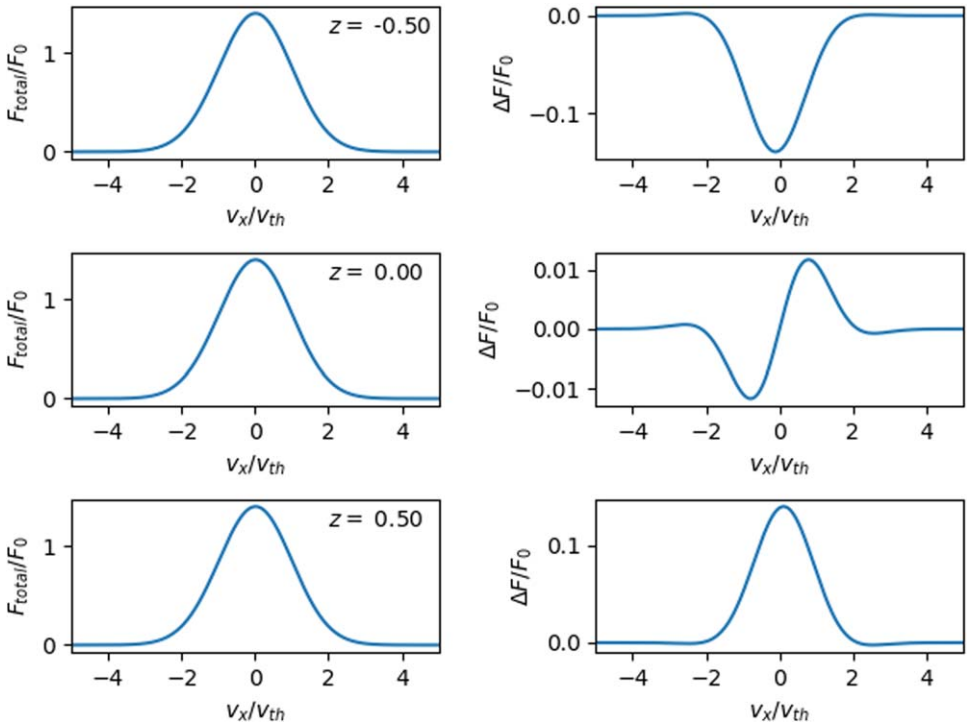

Figure 5. Same plots as in Figure 4, but for the ions. The only noticeable difference to the plots for the electrons is the larger amplitude of ΔF_i at $z = 0$ and the symmetry reversal of its minimum and maximum values.

and temperature that closely resemble those found in the observations.

The work presented in this paper could be further extended in a number of ways. For example, instead of using the distribution functions of Harrison & Neukirch (2009a) as F_{0s}, one can in principle choose any other particle distribution function giving rise to the same magnetic field profile. While the distribution functions used for F_{0s} in this paper always lead to an equilibrium with plasma $\beta > 1$ as well as spatially constant density and temperature profiles, other distribution functions allow for values of plasma $\beta < 1$ (e.g., Allanson et al. 2015, 2016; Wilson et al. 2018) or for additional

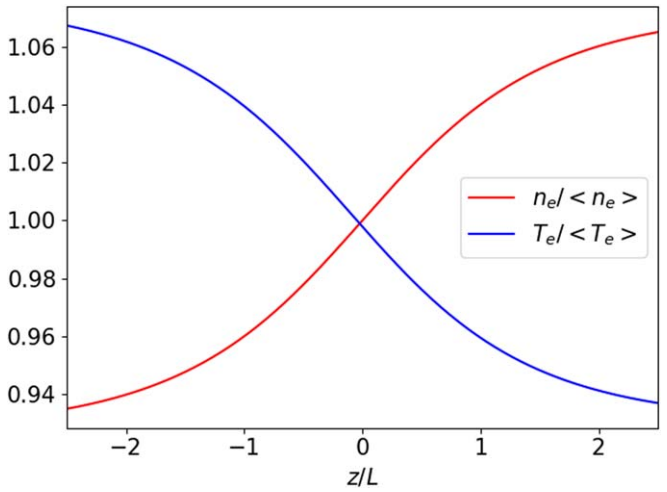

Figure 6. Example of asymmetric density and temperature profiles resulting from the theoretical models ($\epsilon = 0.05$).

symmetric variations in the particle density and temperature (e.g., Kolotkov et al. 2015).

Another possible extension of the work presented here relates to the specific and relatively simple form for ΔF_s that we have used. This form for ΔF_s is just one example taken from a family of possible ΔF_s; other examples include $\Delta F_s \propto \sin(K_s p_{xs}) g_s(H_s)$ and $\Delta F_s \propto \exp(K_s p_{xs}) g_s(H_s)$ (with $\int v_x^2 g_s(H_s) d^3\boldsymbol{v} = 0$ and K_s a model dependent constant).

It is also important to point out that within the same class of particle velocity distribution functions one can develop models of force-free current sheets with symmetric density profiles having either maximum or minimum in center of the current sheet (similar to models of Kolotkov et al. 2015). The symmetric profiles of the plasma density are obtained for distribution functions for which $\Delta n_s(A_x)$ is an even function of $_{Ax}$. The additional population should not contribute to the current density and the simplest choice of such particle distribution functions is $\Delta F_s = g_s(H_s)(\beta_e u_0 p_{xs})^2$, where $g_s(H_s)$ should again satisfy the condition $\int v_x^2 g_s(H_s) d^3\boldsymbol{v} = 0$. For the example distribution function given above, using the same $g_s(H_s)$ that was used in Section 3 the plasma density is as $n_s = n_0(1 + \epsilon 4A_x^2/B_0^2 L^2)$. As $_{Ax}(z)$ is an odd function of z, $A_x^2(z)$ is an even function of z and the density profile is symmetric with respect to the current sheet center.

The self-consistent kinetic current sheet models presented here could, for example, be used as initial conditions for future analyses of collisionless kinetic processes involving tangential discontinuities in the solar wind plasma.

The authors would like to thank the referee for very useful and constructive comments that helped to improve the paper.

T.N. acknowledges financial support by the UK's Science and Technology Facilities Council (STFC) via Consolidated Grant ST/S000402/1. O.A. was supported by the Natural Environment Research Council (NERC) Highlight Topic Grant #NE/P017274/1 (Rad-Sat).

ARTEMIS data analysis was supported by NASA Grant NNX16AF84G and NASA contract NAS5-02099. We would like to thank the following people specifically: C. W. Carlson and J. P. McFadden for use of ESA data; K. H. Glassmeier, U. Auster, and W. Baumjohann for the use of FGM data provided under the lead of the Technical University of Braunschweig; and with financial support through the German Ministry for Economy and Technology and the German Aerospace Center (DLR) under contract 50 OC 0302. THEMIS data (ESA and FGM) were obtained from http://themis.ssl. berkeley.edu/. Data access and processing were done using SPEDAS V3.1; see Angelopoulos et al. (2019).

ORCID iDs

T. Neukirch https://orcid.org/0000-0002-7597-4980
I. Y. Vasko https://orcid.org/0000-0002-4974-4786
A. V. Artemyev https://orcid.org/0000-0001-8823-4474
O. Allanson https://orcid.org/0000-0003-2353-8586

References

Allanson, O., Neukirch, T., Troscheit, S., & Wilson, F. 2016, JPlPh, 82, 905820306
Allanson, O., Neukirch, T., Wilson, F., & Troscheit, S. 2015, PhPl, 22, 102116
Allanson, O., Troscheit, S., & Neukirch, T. 2018, JApMa, 83, 849
Angelopoulos, V. 2011, SSRv, 165, 3
Angelopoulos, V., Cruce, P., Drozdov, A., et al. 2019, SSRv, 215, 9
Artemyev, A. V. 2011, PhPl, 18, 022104
Artemyev, A. V., Angelopoulos, V., Halekas, J. S., et al. 2018, ApJ, 859, 95
Artemyev, A. V., Angelopoulos, V., & Vasko, I.-Y. 2019a, JGRA, 124, 3858
Artemyev, A. V., Angelopoulos, V., Vasko, I.-Y., et al. 2019b, GeoRL, 46, 1185
Auster, H. U., Glassmeier, K. H., Magnes, W., et al. 2008, SSRv, 141, 235
Bobrova, N. A., & Syrovatskiĭ, S. I. 1979, JETPL, 30, 535
Burlaga, L. F., Lemaire, J. F., & Turner, J. M. 1977, JGR, 82, 3191
Cranmer, S. R., Matthaeus, W. H., Breech, B. A., & Kasper, J. C. 2009, ApJ, 702, 1604
De Keyser, J., Echim, M., & Roth, M. 2013, AnGeo, 31, 1297
De Keyser, J., & Roth, M. 1997, in ESA Special Publication 415, Correlated Phenomena at the Sun, in the Heliosphere and in Geospace, ed. A. Wilson (Noordwijk: ESA), 75
De Keyser, J., Roth, M., Lemaire, J., et al. 1996, SoPh, 166, 415
De Keyser, J., Roth, M., & Söding, A. 1998, GeoRL, 25, 2649
De Keyser, J., Roth, M., Tsurutani, B. T., Ho, C. M., & Phillips, J. L. 1997, A&A, 321, 945
Franci, L., Cerri, S. S., Califano, F., et al. 2017, ApJL, 850, L16
Gardner, C. S. 1963, PhFl, 6, 839
Gosling, J. T. 2012, SSRv, 172, 187
Greco, A., Matthaeus, W. H., Servidio, S., Chuychai, P., & Dmitruk, P. 2009, ApJL, 691, L111
Greco, A., Perri, S., Servidio, S., Yordanova, E., & Veltri, P. 2016, ApJL, 823, L39
Harris, E. 1962, Nuovo Cimento, 23, 115
Harrison, M. G., & Neukirch, T. 2009a, PhRvL, 102, 135003
Harrison, M. G., & Neukirch, T. 2009b, PhPl, 16, 022106
Horbury, T. S., Burgess, D., Fränz, M., & Owen, C. J. 2001, GeoRL, 28, 677
Knetter, T., Neubauer, F. M., Horbury, T., & Balogh, A. 2004, JGR, 109, A06102
Kocharovsky, V. V., Kocharovsky, V. V., & Martyanov, V. J. 2010, PhRvL, 104, 215002
Kolotkov, D. Y., Vasko, I. Y., & Nakariakov, V. M. 2015, PhPl, 22, 112902
Krall, N. A., & Trivelpiece, A. W. 1973, Principles of Plasma Physics (New York: McGraw-Hill)
Lemaire, J., & Burlaga, L. F. 1976, Ap&SS, 45, 303
Lepping, R. P. 1986, AdSpR, 6, 269
Lu, S., Angelopoulos, V., Artemyev, A. V., et al. 2019a, ApJ, 878, 109
Lu, S., Artemyev, A. V., Angelopoulos, V., et al. 2019b, JGRA, 124, 1052
Mallet, A., Schekochihin, A. A., & Chandran, B. D. G. 2017, MNRAS, 468, 4862
McFadden, J. P., Carlson, C. W., Larson, D., et al. 2008, SSRv, 141, 277
Medvedev, M. V., Diamond, P. H., Shevchenko, V. I., & Galinsky, V. L. 1997, PhRvL, 78, 4934
Neugebauer, M. 2006, JGR, 111, A04103
Neukirch, T., Wilson, F., & Allanson, O. 2018, PPCF, 60, 014008
Neukirch, T., Wilson, F., & Harrison, M. G. 2009, PhPl, 16, 122102
Osman, K. T., Matthaeus, W. H., Greco, A., & Servidio, S. 2011, ApJL, 727, L11
Panov, E. V., Artemyev, A. V., Nakamura, R., & Baumjohann, W. 2011, JGR, 116, A12204

Paschmann, G., Haaland, S., Sonnerup, B., & Knetter, T. 2013, AnGeo, 31, 871
Podesta, J. J. 2017, JGRA, 122, 2795
Pucci, F., Velli, M., Tenerani, A., & Del Sarto, D. 2018, PhPl, 25, 032113
Pulupa, M. P., Salem, C., Phan, T. D., Gosling, J. T., & Bale, S. D. 2014, ApJL, 791, L17
Roth, M., De Keyser, J., & Kuznetsova, M. M. 1996, SSRv, 76, 251
Sonnerup, B. U. Ö., & Cahill, L. J., Jr. 1968, JGR, 73, 1757
Sonnerup, B. U. Ö., & Scheible, M. 2000, in ESA Special Publication 449, ISSI Book on Analysis Methods for Multi-Spacecraft Data, ed. G. Paschmann & P. Daly (Noordwijk: ESA), 185
Schindler, K. 2007, Physics of Space Plasma Activity (Cambridge: Cambridge Univ. Press)
Tsurutani, B. T., & Smith, E. J. 1974, JGR, 79, 118
Tsurutani, B. T., & Smith, E. J. 1979, JGR, 84, 2773
Vasko, I. Y., Artemyev, A. V., Petrukovich, A. A., & Malova, H. V. 2014, AnGeo, 32, 1349
Vech, D., Mallet, A., Klein, K. G., & Kasper, J. C. 2018, ApJL, 855, L27
Wilson, F., & Neukirch, T. 2011, PhPl, 18, 082108
Wilson, F., Neukirch, T., & Allanson, O. 2017, PhPl, 24, 092105
Wilson, F., Neukirch, T., & Allanson, O. 2018, JPlPh, 84, 905840309
Wilson, F., Neukirch, T., Hesse, M., Harrison, M. G., & Stark, C. R. 2016, PhPl, 23, 032302
Yoon, P. H., & Lui, A. T. Y. 2004, JGR, 109, 11213